Multi-Frequency Lock-In Detection with Non-Sinusoidal References

Peter M. Hintenaus, *Member, IEEE,* Horst Trinker

***Abstract*—We present a lock-in detection scheme, which simultaneously computes the amplitude and phase of several signals using non-sinusoidal references that have odd harmonics only. By stating constraints on the frequencies of the references and on the measurement time, we guarantee perfect discrimination of the sources. Using square-wave references we simplify the lock-in algorithm, rendering it suitable to an implementation directly in logic.**

Furthermore, we apply this scheme to the design of a moisture sensor for industrial real-time measurement applications.

***Index Terms*—Digital lock-in detection, lock-in amplifier, multi-frequency non-sinusoidal lock-in, spectroscopy, moisture sensor, least squares regression moisture model**

I. Introduction

THE lock-in amplifier approach, introduced by R. H. Dicke in [1], imposes a periodic reference signal onto a system via a source. A detector picks up the response of the system. The lock-in amplifier multiplies the output of the detector with the reference on the one hand and a phase-shifted version of the reference on the other. It low-pass filters both products to compute estimates for the part of the response of the system that is in-phase with the reference as well as for the part that is in quadrature. The spectral sensitivity of such an amplifier consists of bands, each centered either on the frequency of the reference itself or on the frequency of one of the harmonics of the reference. The bands are twice as wide as the bandwidth of the low-pass filters. Narrowing the bandwidth of the low-pass filters allows one to construct a device that extracts amplitude and phase of weak responses buried in noise [2].

Lock-in amplifiers, which generate the reference internally, are used with sources like light emitting diodes that can be modulated rapidly [3]–[10]. Restelli *et al.* describe an implementation in logic using an internally generated sinusoidal reference [11].

Lock-in amplifiers, which allow an external reference, are used with sources like thermal radiators that cannot be modulated easily. In such an application some sort of mechanical chopper modulates the output of the source. A lock-in amplifier for this type of system typically uses a phase-locked loop to synchronize an internally generated reference to its reference input [8], [12]–[14]. For an implementation using a digital signal processor see [15].

Early digital lock-in amplifiers [6], [16], [17] employ a voltage-to-frequency converter and a counter for analog to digital conversion, see e.g. [18]. Such schemes lend themselves both to architectures with internal as well as external reference signals.

Multi-channel lock-in amplification comes in two flavors. In the first variant – the multi-detector lock-in – a single reference signal is imposed by one or several sources onto the system. Several detectors pick up different physical responses of the system simultaneously. The amplifier multiplies each detector signal with the reference and low-pass filters the products. Both systems with an internal reference [19], [20] and with external reference [21] are used. In the second – multi-frequency lock-in – several reference signals are imposed via several sources onto the system and a single detector picks up the response. The part of the response of the system that can be attributed to a single source is computed by multiplying the source's reference with the response and low-pass filtering. To achieve perfect separation, one has to choose the type of reference signals, the frequencies of the references, and the low-pass filters carefully. Hielscher *et al.* use multi-frequency lock-in amplification for optical tomography of human tissues [22]. In optical tomography systems Flexman, Hielscher *et al.* use a combination of both approaches resulting in a system that applies several references to several sources and picks up the responses with several detectors [23], [24].

In [25] all low-pass filters are averaging filters with equal-valued coefficients. All filters have the same averaging time. Each sinusoidal reference is averaged over an integer number of periods. In this paper we too use averaging filters. We define a large class of non-sinusoidal references, which includes square-waves. For this class we give a set of design rules for the cycle-times of the references and for the time of a complete measurement. Using square-waves as references we present a simplified version of the multi-frequency lock-in algorithm, which avoids the multiplication operations and the lookup tables for the references. When building systems with a moderately large number of sources, this version lends itself to an implementation directly in logic.

In the second part of this work we apply our multi-frequency lock-in method to the measurement of the moisture content of paper. The sensor we built employs three infrared sources and a single detector. The moisture content of products is an important parameter, e.g. in cellulose manufacturing, in the production of pharmaceutics or in food analysis [26]–[29]. See [30] for an overview of near-infrared based methods. Direct measurement of moisture content based on weighing

P. Hintenaus is with the Department of Computer Sciences, University of Salzburg, 5020 Salzburg, Austria, e-mail: peter.hintenaus@cs.uni-salzburg.at

H. Trinker is with the Department of Computer Sciences, University of Salzburg, 5020 Salzburg, Austria, e-mail: horst.trinker@cs.uni-salzburg.at

This work was partially supported by the Christian Doppler Laboratory *Embedded Software Systems*, University of Salzburg, and the Austrian research funding association (*FFG*) under the scope of the COMET program within the research network "*Process Analytical Chemistry (PAC)*" (contract # 825340). This programme is promoted by BMVIT, BMWFJ and the federal state of Upper Austria.

and drying ("LOD" – loss on drying) serves as reference method (cf. [27], [30]).

Indirect methods based on infrared light, on electrical conductivity or on ultrasound, see e.g. [31] [30, p. 4], are non-invasive, fast and easy to handle with respect to sample preparation [32]. Infrared based methods in particular are well-suited for in-line measurement of moisture content [33]. As the indirect methods do not produce a measure of the moisture content directly one uses regression methods such as partial least squares (PLS) [34], in order to train a model to estimate the actual moisture content.

This work is organized as follows: In the first part we derive the equations to be used for multi-frequency lock-in detection using non-sinusoidal references and discuss implementation issues. In the second part we describe the sensor we developed, explain the experimental setup for collecting the training data and derive a partial least squares model for the prediction of moisture content within paper.

II. Multi-Frequency Lock-In Detection

A. Statement of the Problem

A target T is subjected to n reference signals $r_1(t), \dots, r_n(t)$ via the sources $S_1, \dots, S_n$. The combined response of T is detected by a single detector D and filtered by the signal conditioning electronics E, resulting in the measurement $M(t)$.

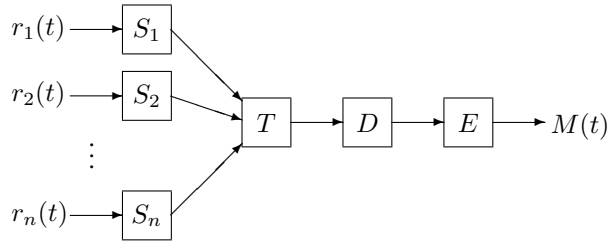

Fig. 1. Diagram of measurement setup with a single detector.

For the sake of simplicity we limit our presentation to systems with a single detector. For systems with several detectors one has to duplicate the signal conditioning electronics and run the lock-in procedure for each detector in parallel.

We assume that, for each $1 \le i \le n$, the combination of the source S_i, the target T, the detector D and the signal-conditioning electronics E forms a linear time-invariant system with impulse response $h_i(t)$. Then the response of this system, the single-channel measurement $m_i(t)$, is the convolution of the reference $r_i(t)$ with the impulse response $h_i(t)$,

$$m_i(t) = (r_i * h_i)(t).$$

Furthermore, we assume that $M(t) = \sum_{i=1}^{n} m_i(t)$.

The problem is (1) to characterize the references $r_1, \dots, r_n$ such that each single-channel measurement $m_i(t)$ can be (partially) reconstructed from $M(t)$ and (2) to provide an efficient procedure for this reconstruction.

B. Non-Sinusoidal References

We consider band-limited non-sinusoidal periodic references $r_1, \dots, r_n$ with commensurate frequencies $f_1, \dots, f_n$. The i-th channel consists of the source S_i, the target and the detector. We know that its steady-state response to a periodic, non-sinusoidal reference r_i with Fourier expansion

$$r_i(t) = \sum_{k=1}^{N_i} A_{ik} \cos(2\pi k f_i t + \varphi_{ik})$$

of frequency $f_i \in \mathbb{Q}^+$ is

$$m_i(t) = \sum_{k=1}^{N_i} B_{ik} \cos(2\pi k f_i t + \varphi_{ik} + \psi_{ik}),$$

for some positive integers $N_1, N_2, \dots$, some amplitudes $B_{i1}, B_{i2}, \dots$ and some phase-shifts $\psi_{i1}, \psi_{i2}, \dots$, because the convolution with h_i is a bounded linear operator (see e.g. [35], [36]).

Let the measurement period τ be an integer multiple of $\frac{1}{f_i}$ for all $1 \le i \le n$. To recover some information about the amplitude as well as the phase of the response, we consider the magnitude of the in-phase part of the response

$$I_i = \int_0^\tau r_i(t)\, m_i(t)\, dt = \frac{\tau}{2} \sum_{k=1}^{N_i} A_{ik} B_{ik} \cos \psi_{ik}$$

and the magnitude of the quadrature part

$$Q_i = \int_0^\tau s_i(t)\, m_i(t)\, dt = \frac{\tau}{2} \sum_{k=1}^{N_i} A_{ik} B_{ik} \cos(\psi_{ik} + \frac{\pi\, k}{2})),$$

where $s_i(t) = r_i(t - \frac{\pi}{2})$ is the signal resulting from shifting r_i by $\frac{\pi}{2}$ forward in time. The amplitude B_{i1} of the response can be estimated by $\sqrt{I_i^2 + Q_i^2}$, and the phase ψ_{i1} by $\arctan(Q_i/I_i)$. As the signal-conditioning electronics of the detector will typically be designed to attenuate the higher harmonics of the response $m_i(t)$, the summands contributed by these harmonics will not disturb I_i and Q_i significantly. Such a low-pass filter with corner frequency f_c and order o attenuates a harmonic with frequency $f_i h > f_c$ by a factor smaller than $\left(\frac{f_c}{f_i h}\right)^o$.

The integral $\int_0^\tau s_1(t)\, \overline{s_2(t)}\, dt$, where s_1 and s_2 are (complex) periodic signals whose frequencies are multiples of $\frac{1}{\tau}$, is the scalar product in the Hilbert space $L^2([0, \tau))$, see e.g. [36]. For real signals the complex conjugate can be dropped, so the real periodic signals s_1 and s_2, whose frequencies are multiples of $\frac{1}{\tau}$, are *orthogonal* if and only if $\int_0^\tau s_1(t)\, s_2(t)\, dt = 0$. Because of the choice of the frequencies of s_1 and s_2 discrete Fourier transforms with duration τ of either s_1 or s_2 do not suffer from spectral leakage.

If the references $r_l(t)$ and $r_m(t)$ have no harmonics in common – more precisely, if $i\, f_l = k\, f_m$ implies that $A_{li} = 0$ or $A_{mk} = 0$ for all positive integers i, k – then $r_l(t)$ and $r_m(t)$ are orthogonal, because the product $r_l(t)\, r_m(t)$ yields no nonzero constant terms as the frequencies of $r_l(t)$ and $r_m(t)$ are commensurate.

To compute the in-phase and out-of-phase magnitudes $I_1, \dots, I_n$ and $Q_1, \dots, Q_n$ from the measurement $M(t)$ we

construct references $r_1(t), \ldots, r_n(t)$, that have pairwise disjoint sets of harmonic frequencies. When using such references, the magnitudes I_i and Q_i can be computed from the measurement $M(t)$ by

$$I_i = \int_0^\tau r_i(t)\, M(t)\, dt,$$

and

$$Q_i = \int_0^\tau s_i(t)\, M(t)\, dt.$$

The assumption, that the response of the target to each source is constant during the measurement period τ is crucial. If the target changes its response to a single source during the measurement period, crosstalk will appear on the other channels despite these responses being constant. Saturation in the signal conditioning electronics or overload of the sensor will produce erroneous results. An implementation has to monitor for these conditions and report them.

C. References Having no Harmonic Frequencies in Common

We first prove a number theoretic observation and then construct suitable references.

Lemma 1: Let $p = 2^e q$ for a positive integer e and a positive odd integer q. For $0 \le i \le e$ let $p'_i = 2^i q_i$, where q_i is a positive odd integer that divides q, and let P_i be the set $\left\{p'_i, \frac{p'_i}{3}, \frac{p'_i}{5}, \ldots\right\}$. Then the sets P_i and P_j are disjoint for $i \neq j$.

Proof: Assume $i > j$. Consider the integer $s = 2^i q_i q_j$. Then the set $P_i = \left\{\frac{s}{q_j}, \frac{s}{3q_j}, \frac{s}{5q_j}, \ldots\right\}$ and the set $P_j = \left\{\frac{s}{2^{i-j}q_i}, \frac{s}{2^{i-j}3q_i}, \frac{s}{2^{i-j}5q_i}, \ldots\right\}$. As the denominators of all fractions in P_i are odd, and the denominators of all fractions in P_j are even, the two sets are disjoint. ∎

For constructing the references we first pick a band-limited function $r(t)$ with periodicity τ that has odd harmonics only. We choose p and $p'_0, \ldots, p'_e$ according to Lemma 1. The functions $g_0(t) = r(t\, p'_0), \ldots, g_e(t) = r(t\, p'_e)$ with frequencies $\frac{p}{\tau\, p'_0}, \ldots, \frac{p}{\tau\, p'_e}$ are pairwise orthogonal. From these candidates we pick references $r_1(t), \ldots, r_n(t)$ with convenient frequencies.

For a digital implementation the measurement $M(t)$ will be sampled. We set the sample period t_s to $\frac{\tau}{p}$. The number of samples in one period of the candidate $g_i(t)$ is p'_i. In order to be able to shift the sampled references by $\pi/2$, p'_i has to be a multiple of 4, so $g_2(t), \ldots, g_e(t)$ remain as candidates for the references. Let p_i be the number of samples in one period of the chosen reference $r_i(t)$. The odd integers q and $q_1, \ldots, q_e$ allow us to place the references into the desired frequency band. This construction bounds the number of references n with $\log_2 p - 1$ from above. This bound is tight for $p = 2^e$.

D. Implementation Issues

In measurement situations, which suffer from wide-band interference, one has make sure, that both the signal conditioning electronics and the analog to digital converters have such a large dynamic range, that the converters are able to resolve the measurement $M(t)$ on top of this overpowering noise without saturation. Low frequency interference occurring typically at the mains frequency or harmonics of it allows for a different approach: When choosing the references $r_1, \ldots, r_n$ and the sample period t_s according to section II-C, the lowest reference frequency can be picked far enough from low-frequency interference. A high-pass filter introduced right after the detector in the detector electronics E in Fig. 2 can use this frequency gap at the cost of a reduced bandwidth in the measurement to eliminate most of the unwanted interference. The amplifier following this filter can provide enough gain to fill the dynamic range of an analog to digital converter of moderate resolution without being overdriven.

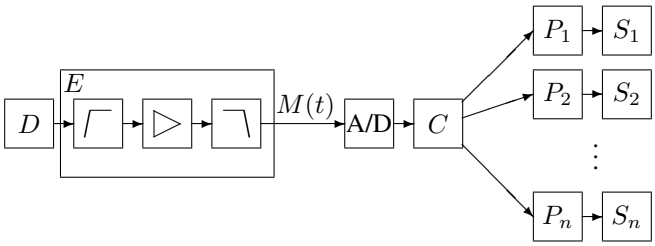

Fig. 2. Architecture of a sensor. The high-pass filter in the detector electronics is optional.

The sampling period t_s has to be chosen short enough to let the low-pass filter that comprises the last stage of the detector electronics pass the highest reference frequency, but attenuate $\frac{1}{2\, t_s}$ in order to satisfy the Shannon-Nyquist criterion (see e.g. [18]) and to prevent aliasing during the analog to digital conversion. According to the design rule for an anti-aliasing filter, the attenuation of the low-pass filter has to be set such that the least-significant bit of the analog to digital converter is not influenced by signal content at $\frac{1}{2\, t_s}$ or above.

In an implementation the analog to digital converter sampling the measurement $M(t)$ will be triggered by a hardware clock periodically with period t_s. In turn, the analog to digital converter will deliver an interrupt to the digital controller C in Fig. 2, whenever a conversion is completed. For processing this interrupt, the procedure DOSAMPLE (Fig. 3) is called with the newly converted sample. The state variables of this procedure have to be initialized before the first call. The accumulators I_i and Q_i have to be set to 0, the counters cI_i and the counter c to 0, and the counters cQ_i to $\frac{3}{4}p_i$. The values of $r(t)$ required for the i-th channel are tabulated in the lookup table ref_i, i.e. $ref_i[j] = r\left(j\frac{p}{p_i}t_s\right)$ for $0 \le j < p_i$. These lookup tables together require $\sum_{i=1}^{n} p_i$ words of storage. Alternatively the references can be stored in a single lookup table ref of length $l' = \mathrm{lcm}(p_1, \ldots, p_n)$, where $ref[j] = r\left(j\frac{p}{l'}t_s\right)$. To extract the values for the i-th reference this table has to be addressed with a stride of $\frac{l'}{p_i}$.

For driving the references $r_1, \ldots, r_n$ to the sources $S_1, \ldots, S_n$ the digital controller activates the power stages $P_1, \ldots, P_n$. The procedure DOSAMPLE, Fig.3, requires $2n$ multiplications, $2n$ additions and $2n$ index updates per run. It uses $4n$ words of memory for accumulators and counters. Computing a single set of results requires $2\,p\,n$ multiplications, $2\,p\,n$ additions and $2\,p\,n$ index updates. Alternatively the problem can be attacked with the Discrete Fourier transform,

```
1: procedure DOSAMPLE(M)
2:     for all i ∈ {1,...,n} do
3:         (I_i, Q_i) ← (I_i + ref_i[cI_i] M, Q_i + ref_i[cQ_i] M)
4:         cI_i ← (cI_i + 1)  mod (p_i)
5:         cQ_i ← (cQ_i + 1)  mod (p_i)
6:         Prepare to write ref_i[cI_i] to source S_i
7:     end for
8:     Update sources S_1,...,S_n simultaneously
9:     c ← c + 1
10:    if c = p then
11:        report I_1,...,I_n, Q_1,...,Q_n
12:        c ← 0
13:        for all i ∈ {1,...,n} do
14:            I_i ← 0, Q_i ← 0
15:        end for
16:    end if
17: end procedure
```

Fig. 3. Procedure DOSAMPLE for processing one sample M.

see e.g. [37]. With $p = 2^e$ and sinusoid references at most $\frac{p}{2} - 1$ channels can be computed. Using the Fast Fourier transform this requires roughly $p(\log_2 p - 3)$ multiplications and $2\,p(\log_2 p - 1)$ additive operations. It uses p words for intermediate results and $\frac{p}{8}$ words for the twiddles.

By using binary signals with a duty cycle of 0.5 for driving the sources and sampled square-waves of amplitude 1 for the references, the computation for a single sample can be simplified considerably: The two multiplications in line 3 of figure 3 can be replaced with a case analysis each, and the tables for the references are not required anymore, see Fig. 4.

The procedure DOSAMPLESQ requires at most $3n$ comparisons, $2n$ additive operations and n counter updates per run. It consumes $3n$ words of memory for accumulators and counters. With an effort of at most $3\,p\,n$ comparisons, $2\,p\,n$ additive operations and $p\,n$ counter updates it produces a single set of results. For $p = 2^e$ the Walsh Hadamard transform is an alternative [38]. As there are only $e - 1$ choices for the frequencies of the Walsh functions of length 2^e that are square waves no additional channels are possible. The Fast Walsh Hadamard transform only requires $p \log_2 p$ additive operations but consumes p words of memory for intermediate results.

For an implementation on a controller without an instruction for multiplication procedure DOSAMPESQ allows for the elimination of the multiplication procedure, reducing the burden placed on the processor, thus the sample period can be kept sufficiently short. Depending on the architecture of the processor, each comparison requires the execution of less than 10 instructions, compared with 150 to 200 for a 32-bit multiplication. When implemented directly in logic, eliminating both, the multipliers and the lookup tables, reduces the gate-count per channel considerably. Two accumulators with arithmetic logic, a counter and two result registers suffice for implementing one channel.

Systems with external references have to make sure that the references exhibit precise frequency relationships. For optical experiments, a chopper with a special wheel, which carries a concentric track with the appropriate number of slots for each channel, placed between the sources of radiation and the target, will provide these relationships. A phase-locked loop locked to the signal derived form an additional track on this wheel can recover the clock for triggering the analog to digital conversion.

```
1: procedure DOSAMPLESQ(M)
2:     for all i ∈ {1,...,n} do
3:         if C_i < p_i/2 then
4:             I_i ← I_i + M
5:         else
6:             I_i ← I_i − M
7:         end if
8:         if p_i/4 ≤ C_i < 3p_i/4 then
9:             Q_i ← Q_i + M
10:        else
11:            Q_i ← Q_i − M
12:        end if
13:        C_i ← (C_i + 1)  mod (p_i)
14:        Prepare to write C_i < p_i/2 to source S_i
15:    end for
16:    Update sources S_1,...,S_n simultaneously
17:    c ← c + 1
18:    if c = p then
19:        report I_1,...,I_n, Q_1,...,Q_n
20:        c ← 0
21:        for all i ∈ {1,...,n} do
22:            I_i ← 0, Q_i ← 0
23:        end for
24:    end if
25: end procedure
```

Fig. 4. Procedure DOSAMPLESQ for processing one sample M using square-wave references.

Method	C	M	A	I
Sinusoidal	$p/2-1$	$2\,p\,n$	$2\,p\,n$	$4n$
FFT, $p = 2^e$	$p/2-1$	$p(\log_2 p - 3)$	$2\,p(\log_2 p - 1)$	p
Odd-harmonics	$e-1$	$2\,p\,n$	$2\,p\,n$	$4n$
Square-wave	$e-1$	0	$2\,p\,n$	$3n$
WHT, $p = 2^e$	$e-1$	0	$p \log_2 p$	p

TABLE I
COMPARISON OF MULTI-FREQUENCY LOCK-IN METHODS, ON-LINE WITH SINUSOIDAL REFERENCES, FAST FOURIER TRANSFORM BASED, REFERENCES WITH ODD HARMONICS ONLY, SQUARE-WAVE REFERENCES AND WALSH HADAMARD TRANSFORM BASED. THE MAXIMUM NUMBER OF CHANNELS IS C, THE NUMBER OF MULTIPLICATIONS IS M, A IS THE NUMBER OF ADDITIONS AND I IS THE NUMBER OF INTERMEDIATE WORDS REQUIRED.

Table I compares five multi-frequency lock-in methods. If the number of channels is less than e using square-wave references is best in terms of resource consumption. For larger numbers of channels the Fast Fourier transform with sinusoidally driven sources is the better method.

E. Experimental Verification

To validate our proposed lock-in scheme we have built a purely electrical simulator with three inputs. The input signals,

gre

Channel	Frequency	Amplitude	Phase
1	2.460 kHz	601.0 mV	52.9°
2	2.236 kHz	633.8 mV	50.8°
3	2.049 kHz	657.0 mV	49.0°

TABLE II
MEASURED FREQUENCIES AND RESPONSES FOR THE FIRST SET OF TESTS. EXCITATION IS SINUSOIDAL WITH AN AMPLITUDE OF 1.0 V PEAK-PEAK.

Test	B_1'	ψ_1'	B_2'	ψ_2'	B_3'	ψ_3'
1	600.7	53.3	**633.8**	51.1	658.5	49.3
2	**601.0**	53.3	noise		noise	
3	noise		**633.8**	51.1	noise	
4	noise		noise		**657.0**	49.3
5	599.9	49.9	**633.8**	47.7	659.6	45.9
6	**601.0**	49.9	noise		noise	
7	noise		**633.8**	47.7	noise	
8	noise		noise		**657.0**	45.9

TABLE III
TESTS WITH ORTHOGONAL REFERENCES, NO CROSSTALK CAN BE OBSERVED.

binary signals with a duty-cycle of 0.5, are provided by a microcontroller, which samples the output with its analog to digital converter and runs the lock-in procedure. The converter has a resolution of 10 bits. Each channel consists of an RC low-pass filter with a corner frequency of 1.69 kHz. An inverting adder adds the filtered and buffered input signals and provides the output. To avoid overdriving the following converter it has a gain of $1/3$.

We first measured the frequencies produced by the microcontroller with an oscilloscope[1]. Then we fed each channel separately with a sine wave with an amplitude of 1.0 V peak to peak, generated by a function generator[2], and measured amplitude and phase of each channels response. For the first set of experiments we set $p_1 = 48$, $p_2 = 44$ and $p_3 = 40$, see table II.

Conservatively estimated, the signal to noise ratio of our setup is better than 75 dB. The different lock-in procedures have different gain. To allow for easy comparisons we picked the amplitude of one channel in each test, indicated in bold face in tables III and V, and scaled it to the measured value. Using the same scale factor we scaled the other two amplitudes. In tables III and V the scaled amplitudes are $B_1', \ldots, B_3'$, and the reported phase shifts are $\psi_1, \ldots, \psi_3$. Results below the noise floor of our simulator are marked with the word "noise".

For the first four tests we used procedure 3 with sinusoidal references. We adjusted the phases of the references slightly to match the phases we measured. In the first test, all three inputs were exercised simultaneously, whereas in tests two to four we exercised a single channel only. For tests five to eight we used procedure 4. Test five exercised all three inputs simultaneously while the remaining tests exercise a single reference each, see table III. When comparing sinusoidal with square-wave references the ratios of the amplitudes match with an error

[1]Agilent MSO7054A
[2]Agilent 33220A

Channel	Frequency	Amplitude	Phase
1	2.236 kHz	633.8 mV	50.8°
2	2.049 kHz	657.0 mV	49.0°
3	1.229 kHz	821.5 mV	34.2°

TABLE IV
MEASURED RESPONSES FOR $p_1 = 44$, $p_2 = 48$ AND $p_3 = 80$. REFERENCES 2 AND 3 ARE NOT ORTHOGONAL.

Test	B_1'	B_2'	B_3'
9	620.4	**657.0**	658.5
10	**633.8**	noise	noise
11	noise	**657.0**	18.7
12	noise	18.1	**821.5**

TABLE V
REFERENCES 2 AND 3 ARE NOT ORTHOGONAL, RESULTING IN CROSSTALK BETWEEN CHANNELS 2 AND 3.

of about 0.5%. While it is possible to tune the phases of the tabulated references in procedure 3, no such possibility exists in procedure 4.

To demonstrate the importance of orthogonal references we ran a second set of tests. We set the periods to $p_1 = 44$, $p_2 = 48$ and $p_3 = 80$, in violation of the construction in section II-C. Table IV contains the measured responses. Test nine in Table V exercises all three channels simultaneously. The computed amplitude for channel 3 is off by about 20%, which is not acceptable. Tests ten to twelve exercise a single channel each. The strong crosstalk between channels 2 and 3 in the last two tests again renders this choice for p_1, p_2 and p_3 unusable.

III. MOISTURE MEASUREMENT

A. The Sensor

Our moisture sensor exploits the strong absorption peak around 1.45 µm, see e.g. [29], [30], in the infrared spectrum of water. It uses three infrared LEDs, S_1 (peak emission wavelength of 1.45 µm)[3], S_2 (1.3 µm)[4], and S_3 (1.65 µm)[5], as sources. Each source has a −3 dB bandwidth of 100 nm. The detector is a InGaAs PIN photodiode[6] with a spectral response range of 0.9 µm − 1.7 µm. The response of the detector peaks at 1.55 µm and tapers off slowly towards shorter wavelengths. At incident light levels below 6 mW the detectors response is essentially linear. Each LED is driven by a software-programmable current source that can be switched on and off. The sampling period was chosen at $t_s = 10.173$ µs, the periods $p_1 = 40$, $p_2 = 44$ and $p_3 = 48$. This choice avoids multiples of the mains frequency for the references and achieves a high enough measurement rate of 18.2 Hz, while consuming about 50% of the computing power available. It results in a nominal switching frequency of 2.4575 kHz for S_1, of 2.234 kHz for S_2, and of 2.0479 kHz for S_3. The closeness of the reference frequencies enables us to use a narrow-band detector electronics.

[3]Hamamatsu L10660-01.
[4]Hamamatsu L10822-01.
[5]Hamamatsu L10823-01.
[6]Hamamatsu G8370-81.

The current from the photodiode is first converted to a voltage by a transimpedance amplifier with a gain of 10 MV/A and a bandwidth of 4.8 kHz. The bandwidth of this amplifier was set to prevent oscillatory behavior. The output of the transimpedance amplifier is filtered by a second-order high-pass filter with a corner frequency of 1 kHz, before being amplified by a software-programmable variable gain $(10 - 2000)$ amplifier. The second-order high-pass filter provides an attenuation of more than 40 dB at twice the mains frequency suppressing interference from e. g. fluorescent light, while passing the detectors response at the sources frequencies undisturbed. A second-order low-pass filter with a corner frequency of 5 kHz completes the signal conditioning electronics. Its output is converted to digital with the sampling period t_s and a resolution of 10 bits. The low-pass filter and the transimpedance amplifier have a combined attenuation of more than 60 dB at the Nyquist frequency, which is adequate for 10 bit resolution. The samples are processed with the algorithm in Figure 3 running on a 32-bit microcontroller[7]. The measurement results are passed to a PC using an USB interface.

B. Measurement Setup and Data Collection

For an empirical experiment, we have chosen three types of paper, A, B and C. Papers A and B weigh about 120 grams per square meter each, while type C weighs about 80 grams per square meter. As the sides of A and B are visually different, we set-up two specimens A_1, B_1 and A_2, B_2 each, A_1 and B_1 for measuring the respective front side, A_2 and B_2 for the back. We prepared the specimens by cutting disks of 140 mm diameter and placed them into culture dishes.

We determine the moisture content of a paper specimen Z ($Z = A_1, A_2, B_1, B_2, C$) by comparing its actual mass Θ_Z with its dry mass Ω_Z. We cured each specimen separately in a microwave oven. Immediately afterwards we measured its dry mass. In general, finding the *exact* dry mass of a paper is hard as wood fibers are very hydrophilic and do not give up water easily (even when dried in an oven), and, moreover, oven-drying not only causes mass loss due to moisture evaporation, but also due to chemical breakdowns resulting from heat exposure [26]. Nevertheless, for our purposes we deem this method exact enough to yield a reliable model as we shall see below.

The relative humidity of Z is given by

$$\eta_Z = \frac{\Theta_Z - \Omega_Z}{\Omega_Z}$$

(cf. also [26]). We measured all masses with an electronic scale[8]. The scale has a maximal weighing range of 1000 g, a reproducibility of 0.01 g and a linearity of ± 0.03 g.

In order to avoid specular reflections, we have chosen a measurement setup such that the beams from the three LEDs hit the target (the five paper specimens) at an angle of about 60°. The LEDs as well as the detector have a typical distance of about 200 mm from the target, which results in an elliptic (almost circular) measurement area on the target with a diameter of about 50 mm. We neglect the exact moisture distribution within the paper specimens because the papers are thin enough and the infrared light penetrates the surface to a certain depth.

[7]The processor has a multiplication instruction, but we did not use it. In this case we gain from eliminating the tabulated references only.

[8]Kern PCB 1000-2 [39].

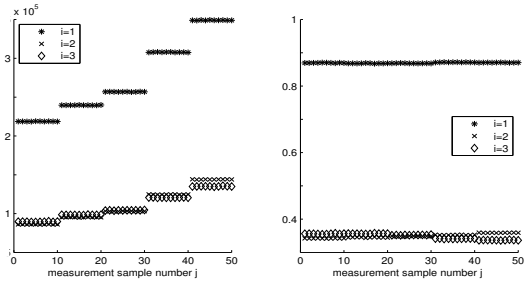

Fig. 5. A single paper specimen with constant moisture content measured from five different positions, ten times in a row for each position. The unnormalized amplitudes ι'_i (left hand side) and the normalized amplitudes ι_i (right hand side), $i = 1, 2, 3$, are plotted on the vertical axes.

We obtained training as well as validation data by moisturizing the five paper specimens and letting them air-dry. During various states of these drying processes we measured the masses of the specimens as well as their infrared responses. For each measurement j of specimen Z we collected the relative humidity $\eta_{Z,j}$ as well as the three amplitudes $\iota'_i = \iota'_{Z,j,i}$ of the responses m_i corresponding to channels $i = 1, 2, 3$.

We repeated the experiments several times on several days yielding $580 \cdot 5 = 2900$ measurement datasets, from which we used 900 datasets (which have been collected in a first series of measurements) for building a moisture model and the remaining 2000 datasets as validation data.

C. A moisture model

By considering the normalized vector $\iota = (\iota_1, \iota_2, \iota_3)$,

$$\iota_i := \frac{\iota'_i}{\sqrt{{\iota'_1}^2 + {\iota'_2}^2 + {\iota'_3}^2}} \quad \text{for } i = 1, 2, 3,$$

instead of $\iota' = (\iota'_1, \iota'_2, \iota'_3)$ we compensate for the dependence of ι' on the distance between sensor and target (see Fig. 5). Due to this normalization step the amplitude vectors $(\iota_{Z,j,1}, \iota_{Z,j,2}, \iota_{Z,j,3}) \in \mathbb{R}^3$ lie on the three-dimensional unit sphere , which is in fact a two-dimensional space. This means that any two components of the vector uniquely determine the third component (up to its sign, which is always positive) in a non-linear way.

Our aim is to build a *linear* model

$$\alpha(\iota) = \beta_0 + \sum_{i=1}^{3} \beta_i \iota_i \tag{1}$$

that predicts the relative humidity η. Thereby, the real-valued parameters $\beta_0, \beta_1, \beta_2$ and β_4 have to be determined such that the prediction error is minimized. For ordinary least squares regression, which we will use, the prediction error calculates as sum of squares of the residuals,

$$\sum_{Z,j} (\alpha(\iota_{Z,j}) - \eta_{Z,j})^2,$$

where the indices Z and j vary over all training samples. Using a linear approach for measuring moisture content has already been successfully applied in combination with infrared-based spectroscopy (see e.g. [30] and the references given there). Nevertheless we face a fair challenge as we are dealing with only three responses instead of several hundreds usually given in spectroscopy.

In general, we cannot assume that a linear approach is able to appropriately model the given data. The coefficient of determination, R^2, which in the case of the linear least squares model (1) can be calculated as the square of Pearson's correlation coefficient between the actual humidities $\eta_{Z,j}$ and the predicted values $\alpha(\iota_{Z,j})$, the indices Z, j again varying over all training samples, is a quality measure for the goodness of fit of the calculated linear model (see e.g. [40], [41]). For our whole training set, consisting of 900 datasets, the R^2 coefficient calculates to 0.927, which means that the linear model roughly covers 93% of the total humidity variation.

There is a general difficulty in determining the exact humidity when a paper specimen is saturated and a thin film of water starts to form on top of the target dominating the response more or less independently of how much more water is put onto the target. Put another way, the measurements become unreliable when humidity gets too high. This particularly concerns our measurement setup using culture dishes, in which water can only evaporate, but not run off. For this reason, we only consider the 1670 samples (590 for model building, 1080 for model verification) satisfying $0 \leq \eta_{Z,j} \leq 1.5$. This is not a real shortcoming, since in many industrial settings, monitoring a drying process will be the prime application – thus the low moisture content has to be measured as precisely as possible. Moreover, if a certain industrial application requires a specific, a-priori known humidity range to be monitored, it is best to take this into account by building a model based on training data within this given humidity range.

In Fig. 6, the relative humidity (vertical axes) is plotted against the amplitude responses of channel $1, 2$ and 3 (horizontal axes) for the training datasets. The 590 datasets within the gray shaded area exhibit a relative humidity of 1.5 or below. Recalculating the linear model from above with respect to this reduced training set yields an improved R^2 coefficient of 0.981, whereas the least squares fitted linear model on all training datasets with a humidity above 1.5 shows a relatively weak R^2 value of 0.384.

The root mean square error (RMSE)

$$\sqrt{\frac{\sum_{Z,j}(\alpha(\iota_{Z,j}) - \eta_{Z,j})^2}{N}} = 0.060,$$

Z and j varying over the $N = 590$ training samples with humidity ≤ 1.5, is a measure for the absolute error that is (at least) to be expected. This value is of practical interest, since for most industrial applications there is a clearly specified demand on the concrete accuracy of predicted process values.

Although a high R^2 is a good measure of linear dependence and a low root mean square error might look promising, it is important to recognize and avoid over-fitting onto the training data, which can effectively be done using cross-validation as well as using separate validation data, which has not been used for building the model (cf. [42, Sec. 7.10]). The R^2 coefficients and root mean square errors of our model with respect to cross-validation and the validation data consisting of 1080 datasets can be found in tableVI[9].

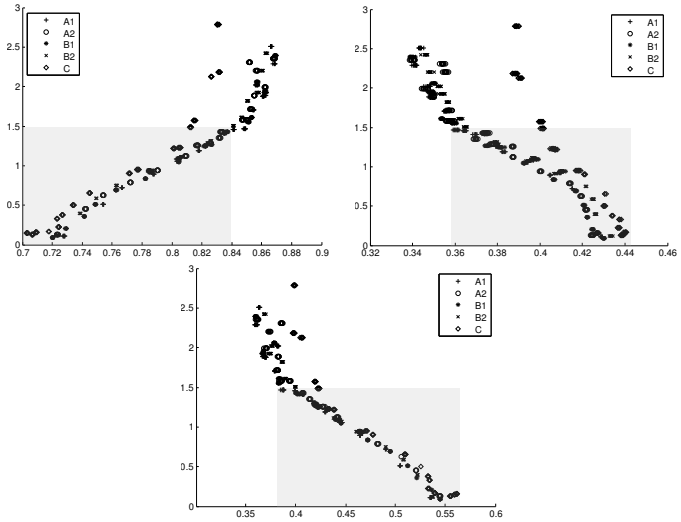

Fig. 6. Relative humidity $\eta_{Z,j}$ (vertical axes) and normalized amplitudes $\iota_{Z,j,i}$ (horizontal axes) of channel $i = 1$ (upper left), $i = 2$ (upper right) and $i = 3$ (bottom), respectively.

	R^2	RMSE
training data	0.981	0.060
cross-validation	0.977	0.065
validation data	0.981	0.062

TABLE VI
COEFFICIENTS OF DETERMINATION R^2 AND ROOT MEAN SQUARE ERRORS OF THE REGRESSION MODEL.

The values reassure the quality of the model and do not reveal any indication of over-fitting.

As stated at the beginning of this section, any two components of the normalized amplitudes vector $\iota = (\iota_1, \iota_2, \iota_3)$, non-linearly determine the third component. Indeed, Pearson's correlation coefficients $r_{i,j}$ between the ι_i and ι_j datasets of the training data, $i, j \in \{1, 2, 3\}$, indicate a very strong relationship: $r_{1,2} = -0.969$, $r_{1,3} = -0.998$ and $r_{2,3} = 0.960$. In cases of high correlation within the input variables, biased regression methods such as principal component regression (PCR) or projection to latent structures (PLS) often lead to more stable predictions by orthogonally transforming the input data into another coordinate system and projecting onto the first few coordinates that show most of the variance in the input data (PCR) or the input data and the reference data (PLS), cf. [42], [44], [45]. We have also calculated a PLS model on the training data. Based on cross-validation, choosing two latent variables (i.e. projecting onto the first two coordinates of the orthogonally transformed input data) yields the best results, but only marginally outperforms the above described ordinary least squares model with slightly better R^2 and RMSE quality parameters that equal those given in table VI for the first

[9]The values have been calculated using *Matlab* by *MathWorks* and *PLS Toolbox* for *Matlab* by *Eigenvector Research* [43].

two decimal places. This result is consistent with the two-dimensional nature of the input data, lying on the three-dimensional unit sphere, but we cannot substantially improve prediction quality using PLS instead of ordinary least squares regression.

IV. Conclusion

We have presented a multi-frequency lock-in method, which uses non-sinusoidal references with odd harmonics. The lock-in method uses constraints on the frequencies of the references and on the measurement time and the locations of the zeros in the frequency response of an averaging filter to guarantee perfect discrimination of the sources. The use of square waves as sources in particular results in an algorithm that can be implemented in hardware without lookup tables and multipliers, using just two adders, two accumulators and one counter per source. We have demonstrated the method with the design of a moisture sensor for industrial in-line measurement applications.

Acknowledgment

The authors would like to thank Peter Porzer for helping us with the presentation of this work. Toni Pölzleitner, Robert Okorn, Wolfgang Pree and Josef Templ provided us with helpful comments. Jürgen Kasberger and Roland Galosch helped us with selecting the sources and the detector. Alwin Pichler provided us with the paper samples. Three anonymous referees helped us improving this work.

References

[1] R. H. Dicke, "The measurement of thermal radiation at microwave frequencies," *Rev. Sci. Instrum*, vol. 17, pp. 286–275, 1946.

[2] D. P. Blair and P. H. Sydenham, "Phase sensitive detection as a means to recover signals buried in noise," *J. Phys. E, Sci. Instrum.*, vol. 8, pp. 621–827, 1975.

[3] X. Wang, "Sensitive digital lock-in amplifier using a personal computer," *Rev. Sci. Instrum.*, vol. 61, pp. 1999–2001, 1990.

[4] L. A. Barragn, J. I. Artigas, R. Alonso, and F. Villuendas, "A modular, low-cost, digital signal processor-based lock-in card for measuring optical attenuation," *Rev. Sci. Instrum.*, vol. 72, pp. 247–251, 2001.

[5] T. I. Oh, J. W. Lee, K. S. Kim, J. S. Lee, and E. J. Wu, "Digital phase-sensitive demodulator for electrical impedance tomography," in *Proc. 25th Annu. Int. Conf.*, Cancun, Mexico, Sep. 2003, pp. 1070–1072.

[6] S. Carrato, G. Paolucci, R. Tommsini, and R. Rosei, "Versatile low-cost digital lock-in amplifier suitable for multichannel phase-sensitive detection," *Rev. Sci. Instrum*, vol. 60, pp. 2257–2259, 1989.

[7] B. W. Pogue, M. Testorf, T. McBride, U. Osterberg, and K. Paulsen, "Instrumentation and design of a frequency-domain diffuse optical tomog- raphy imager for breast cancer detection," *Opt. Express*, vol. 1, pp. 391–403, 1997.

[8] P. K. Dixon and L. Wu, "Broadband digital lock-in amplifier techniques," *Rev. Sci. Instrum*, vol. 60, pp. 3329–3336, 1989.

[9] R. Pei, A. Velichko, Y. Jiang, Z. Hong, M. Katayama, and T. Coombs, "High-precision digital lock-in measurements of critical current and ac loss in hts 2g-tapes," in *SICE Annual Conference, 2008*, aug. 2008, pp. 3147 –3150.

[10] Z. Liu, L. Zhu, A. Koffman, B. C. Waltrip, and Y. Wang, "Digital lock-in amplifier for precision audio frequency bridge," in *Conference on Precision Electromagnetic Measurements (CPEM), 2012*, july 2012, pp. 586–587.

[11] A. Restelli, R. Abbiati, and A. Geraci, "Digital field programmable gate array-based lock-in amplifier for high-performance photon counting applications," *Review of Scientific Instruments*, vol. 76, no. 9, pp. 1–8, sep 2005.

[12] R. Alonso, F. Villuendas, J. Borja, L. A. Barragan, and I. Salinas, "Low-cost, digital lock-in module with external reference for coating glass transmission/reflection spectrophotometer," *Meas. Sci. Technol.*, vol. 14, pp. 551–557, 2003.

[13] F. Barone, E. Calloni, L. DiFiore, A. Grado, L. Milano, and G. G. Russo, "High-performance modular digital lock-in amplifier," *Rev. Sci. Instrum.*, vol. 66, pp. 3697–3702, 1995.

[14] R. M. Josephs, D. S. Compton, and C. S. Krafft, "Application of digital signal processing to vibrating sample magnetometry," *IEEE Trans. Magn.*, vol. MAG-23, pp. 241–244, 1987.

[15] X. Han, P. Ding, J. Xie, J. Shi, and L. Li, "Precise measurement of the inductance and resistance of a pulsed field magnet based on digital lock-in technique," *IEEE Trans. Appl. Supercond.*, vol. 22, 2012.

[16] E. D. Morris and H. S. Johnston, "Digital phase sensitive detector," *Rev. Sci. Instrum*, vol. 39, pp. 620–621, 1968.

[17] S. Cova, A. Longoni, and I. Freitas, "Versatile digital lock-in detection technique: Application to spectrofluorometry and other fields," *Rev. Sci. Instrum*, vol. 50, pp. 296–301, 1979.

[18] W. Kester (editor) and Analog Devices Inc. Engineering, *Data Conversion Handbook*. Amsterdam-London: Elsevier-Newnes, 2005. [Online]. Available: http://www.analog.com/library/analogDialogue/archives/39-06/data_conversion_handbook.htm

[19] P.-A. Probst and A. Jaquier, "Multiple-channel digital lock-in amplifier with ppm resolution," *Rev. Sci. Instrum.*, vol. 65, pp. 747–750, 1994.

[20] A. Albertini and W. Kleeman, "Analogue and digital lock-in techniques for very-low-frequency impedance spectroscopy," *Meas. Sci. Technol.*, vol. 8, pp. 666–672, 1997.

[21] G. Machel and M. von Ortenberg, "A digital lock-in-technique for pulsed magnetic field experiments," *Physica B*, vol. 211, pp. 355–359, 1995.

[22] C. H. Schmitz, M. Locker, J. M. Lasker, A. H. Hielscher, and R. L. Barbour, "Instrumentation for fast functional optical tomography," *Rev. Sci. Instrum*, vol. 73, pp. 429–439, 2002.

[23] M. L. Flexman, M. A. Khalil, R. Al Abdi, H. K. Kim, C. J. Fong, E. Desperito, D. L. Hershman, R. L. Barbour, and A. H. Hielscher, "Digital optical tomography system for dynamic breast imaging," *Journal of Biomedical Optics*, vol. 16, pp. 1–16, 2011.

[24] M. L. Flexman, H. K. Kim, R. Stoll, M. A. Khalil, C. J. Fong, and A. H. Hielscher, "A wireless handheld probe with spectrally constrained evolution strategies for diffuse optical imaging of tissue," *Review of Scientific Instruments*, vol. 83, no. 3, pp. 1–8, 2012.

[25] J. Masciotti, J. Lasker, and A. Hielscher, "Digital lock-in detection for discriminating multiple modulation frequencies with high accuracy and computational efficiency," *IEEE Trans. Instrum. Meas.*, vol. 57, pp. 182–189, 2008.

[26] D. R. Roisum, "Moisture effects on webs and rolls," *Tappi Journal*, vol. 76, pp. 129–137, 1993.

[27] O. Berntsson, G. Zackrisson, and G. Östling, "Determination of moisture in hard gelatin capsules using near-infrared spectroscopy: applications to at-line process control of pharmaceutics," *J. Pharm. Biomed. Anal.*, vol. 15, pp. 895–900, 1997.

[28] S. S. Nielsen, *Food Analysis*. New York - Dordrecht - Heidelberg - London: Springer, 2010.

[29] H. Büning-Pfaue, "Analysis of water in food by near infrared spectroscopy," *Food Chem.*, vol. 82, pp. 107–115, 2003.

[30] S. Groß, "Multivariate Korrektur des Temperatureinflusses in der NIR-spektroskopischen Materialfeuchtebestimmung," PhD thesis, University of Göttingen, 2009. [Online]. Available: http://webdoc.sub.gwdg.de/diss/2009/gross/gross.pdf

[31] K. Kupfer, *Materialfeuchtemessung: Grundlagen, Messverfahren, Applikationen, Normen*. expert-Verlag, 1997.

[32] W. F. McClure, "Near-infrared spectroscopy: The giant is running strong," *Anal. Chem.*, vol. 66, pp. 43A–53A, 1994.

[33] E. Wüst, A. Fehrmann, A. Hoffmann, and L. Rudzik, "In-line measurement of high moisture products," in *Near infrared spectroscopy: The Future Waves*. Montral: NIR Publications, 1995.

[34] S. de Jong, "Simpls: an alternative approach to partial least squares regression," *Chemometrics and Intelligent Laboratory Systems*, vol. 18, pp. 351–363, 1993.

[35] M. Bellanger, *Digital Processing of Signals: Theory and Practice*. Chichester: John Wiley & Sons, 2000.

[36] J. B. Conway, *A course in functional analysis*, 2nd ed., ser. Graduate Texts in Mathematics. New York: Springer-Verlag, 1990.

[37] A. V. Oppenheim and R. Schafer, *Digital Signal Processing*. Prentice-Hall, 1975.

[38] J. Shanks, "Computation of the fast walsh-fourier transform," *Computers, IEEE Transactions on*, vol. C-18, no. 5, pp. 457 – 459, may 1969.

[39] Kern & Sohn GmbH. [Online]. Available: http://www.kern-sohn.com

[40] N. J. D. Nagelkerke, “A note on a general definition of the coefficient of determination,” *Biometrika*, vol. 78, no. 3, pp. 691–692, 1991. [Online]. Available: http://dx.doi.org/10.1093/biomet/78.3.691

[41] C. R. Rao, *Linear statistical inference and its applications*, 2nd ed. John Wiley & Sons, New York-London-Sydney, 1973, wiley Series in Probability and Mathematical Statistics.

[42] T. Hastie, R. Tibshirani, and J. Friedman, *The Elements of Statistical Learning: Data Mining, Inference, and Prediction*, 2nd ed. New York: Springer-Verlag, 2009.

[43] B. M. Wise, J. M. Shaver, N. B. Gallagher, W. Windig, R. Bro, and R. S. Koch, *Chemometrics Tutorial for PLS_Toolbox and Solo*. Wenatchee: Eigenvector Research, Inc., 2006. [Online]. Available: http://www.eigenvector.com

[44] S. Wold, H. Wold, W. J. Dunn, and A. Ruhe, “The collinearity problem in linear regression. The partial least squares (PLS) approach to generalized inverses,” *Siam J. Sci. Stat. Comput.*, vol. 5, pp. 735–743, 1984.

[45] H. Abdi, “Partial least square regression, projection on latent structure regression, PLS-Regression,” *Wiley Interdisciplinary Reviews: Computational Statistics*, vol. 2, pp. 97–106, 2010.

Peter Hintenaus received a master (1986) and a PhD (1989) in Computer Science both from the Universiy of Linz, Austria.

From 1989 to 1993 he held a position as Assistant Professor in Computer Science at Kent State University doing research in Computer Algebra. For two years till 1995 he was self-employed writing Software for the generation of tool-paths for milling. After spending a year at Nycomed Pharma in Linz he joined FH Joanneum in 1996, teaching Computer Science in an electronics course. While at FH Joanneum he was involved in the design of several electronic instruments, from motor-drives to long-term ECG devices. Around 1998 he became involved into the development of a Fourier Infrared Spectrometer for process monitoring applications. In 2006 he co-founded I-RED GmbH, which produces FTIR instrumentation. Since 2008 he holds the position of an Assistant Professor in the Department of Computer Science at the University of Salzburg.

Horst Trinker received a master (2007) and a PhD (2010) in Mathematics from the University of Salzburg, Austria.

From 2006 until 2009 he worked as a research assistant at the Department of Mathematics, where he still teaches as an external lecturer. Since 2010, he works as a researcher at the Department of Computer Science of the University of Salzburg.